journal of the mechanical behavior of biomedical materials 135 (2022) 105413

Contents lists available at ScienceDirect

Journal of the Mechanical Behavior of Biomedical Materials

journal homepage: www.elsevier.com/locate/jmbbm

Research paper

Pre-strains and buckling in mechanosensitivity of contractile cells and focal adhesions: A tensegrity model

E. Benvenuti [a,*], G.A. Reho [a], S. Palumbo [b], M. Fraldi [b,*]

[a] Engineering Department, University of Ferrara, Italy
[b] Department of Structures for Engineering and Architecture, University of Napoli Federico II, Italy

ARTICLE INFO

Keywords:
Cell mechanobiology
Focal adhesion growth
Cellular tensegrity
Nonlinear elasticity

ABSTRACT

We demonstrate that several key aspects of the contractile activity of a cell interacting with the substrate can be captured by means of a non linear elastic tensegrity mechanical system made of a tensile element in parallel with a buckling-prone component, and exchanging forces with the surroundings through an extracellular matrix-focal adhesion complex. Mechanosensitivity of the focal adhesion plaque is triggered by pre-strain-driven buckling of the system induced either by pre-contraction or pre-polymerization of the constituents. The impact of pre-polymerization on the mechanical force and the implications of using linear and nonlinear elasticity for the focal adhesion plaque are assessed.

1. Introduction

Contractile systems occurring at both subcellular and extracellular levels are key to several important phenomena, such as cells locomotion on the extracellular matrix (ECM) and focal adhesion development. This contribution demonstrates the major features of a contractile tensegrity model based on a buckling-prone pre-polymerized component in parallel with a pre-contracted tensile component. These components incrementally respond to inelastic pre-strains with nonlinear elastic deformations. The model is used to analytically investigate the mechanical force developed by a pre-contracted actomyosin fibers bundle in parallel with a pre-polymerized micro-tubule. The expression of the mechanical force is used to obtain the growth rate of the focal adhesion plaque.

The cytoskeleton of non-muscle cells is often modeled as an ensemble of actomyosin networks, composed of many parallel actin and myosin filaments (Kreis and Birchmeier, 1980) linked to microtubules. Microtubules are tubulin polymers that mechanically stabilize the cell shape acting as compressive struts that resist both actomyosin contractile forces and their own polymerization forces (Bicek et al., 2009). Known to promote focal adhesion disassembly (Bershadsky et al., 2006), microtubules may elongate, for instance, by addition of bent guanosine triphosphate tubulin to the tips of curving protofilaments (Gudimchuk et al., 2020). On the other hand, contraction or elongation of an actomyosin system are induced from active tensile forces resulting from the sliding interaction via cross-bridge cycling between actin and myosin (Deshpande et al., 2006).

In eukaryotic cells, the cytoskeleton is then physically linked to the extracellular substrate through the focal adhesions generated by trans-membrane receptors of the integrin family and a large set of adaptor proteins (Wehrle-Haller and Imhof, 2002). Focal adhesions mechanically transduce the signals coming from the cytoskeleton into forces that pull forward the cell and regulate its migration on the substrate. The generated pulling forces depend, among others, on substrate mechanical stiffness, though it is not clear whether this process is stress- or strain-driven (Janmey et al., 2020).

Mechanosensitivity of the cell–ECM interaction has been thoroughly investigated from the analytical standpoint (Schwarz and Safran, 2013; He et al., 2014; Jansen et al., 2015). In particular, structural models both of discrete and continuum type have been exploited to identify the influence of the stiffness of the ECM on cells locomotion and to highlight the mechanism of anchorage of focal adhesions to the substrate. Among others, He et al. (2014) modeled the cell–substrate system as a pre-strained elastic disk attached to an elastic substrate via molecular bonds at the interface. They report traction forces to increase with the substrate stiffness and to asymptotically tend to a constant value for progressively stiff substrates. In this regard, evidences are controversial (Yip et al., 2013). Most experimental and theoretical studies indicate that traction forces increase with substrate stiffness (Lo et al., 2000; Cao et al., 2015). However, other contributions detected an opposite trend for certain cells type (Bangasser et al., 2013). For instance, a stochastic model of myosin motor as a force transmission system (Chan and Odde, 2008) suggested that two distinct regimes can

* Corresponding authors.
E-mail addresses: elena.benvenuti@unife.it (E. Benvenuti), massimiliano.fraldi@unina.it (M. Fraldi).

https://doi.org/10.1016/j.jmbbm.2022.105413
Received 17 June 2022; Received in revised form 4 August 2022; Accepted 5 August 2022
Available online 20 August 2022

arise depending on the substrate stiffness, one with low traction forces on stiff substrates and another one with higher traction forces on soft substrates.

In the vast state-of-the-art literature concerning biophysical and mechanical models of the cell behavior, the so-called dipole model of the contractile actomyosin unit plays a significant role. It consists of two equal and opposite forces separated by a micro- or nano-scale distance (Schwarz and Safran, 2013). When continuously distributed, dipoles give rise to a coarse-grained force density whose gradient induces the net force acting on the cell. Other discrete models replicate the functioning of the actomyosin motor by means of lumped parameters systems based on suitable configurations of springs, dashpots and contractile elements that can be combined either in series or in parallel. Well known examples are the two-parameters Maxwell model and three-parameters elements Hill model for muscles (Cowin and Doty, 2007). More complex discrete models have been also proposed, such as discrete stochastic models with frictional springs simulating the cell–ECM interface (Chan and Odde, 2008). Cao et al. (2015) proposed a lumped model where springs representing the stiffness of the substrate and the nucleus are put in series with a system comprehensive of a contractile element, representing the actomyosin complex, in parallel with a spring, modeling cell elasticity.

Experiments have highlighted that focal adhesions undergo a three-folded turnover process made of an assembly stage, when the focal adhesion plaque increases in size and intensity, a disassembly stage, as the intensity decreases, and the stage in between, during which focal adhesions neither assemble nor disassemble (Stehbens and Wittmann, 2014). The fact that this assembly/disassembly process is sensitive to cytoskeleton tension is widely accepted in the state-of-the-art literature (Kaverina et al., 2002; Chrzanowska-Wodnicka and Burridge, 1996; Stamenović and Ingber, 2009; Shemesh et al., 2005; Cao et al., 2015) and can be experimentally detected (Hirata et al., 2008). Using thermodynamics laws, it is possible to show that the effect of the mechanical force transduced from the cell to the focal adhesion plaque tends to decrease the chemical potential of the aggregated plaque monomers (Hill and Kirschner, 1982). This means that self-assembly of the proteins of the plaque is promoted when the cell exerts pulling forces and inhibited when these forces are relaxed.

The conviction that microtubules are prone to buckling is solid (Coughlin and Stamenović, 1997; Wang et al., 2001; Leijnse et al., 2014; Soheilypour et al., 2015). Tensegrity models capture the mechanical interaction among tensed cables and non-interconnected compressed bars, by also accounting for relevant buckling events possibly undergone by the latter. This property was leveraged to simulate several features of biological systems, including the complex mechanisms regulating the mechanical behavior of the actomyosin complex and the anchorage of actin tubules to the substrate (Wang et al., 2001; Stamenović and Ingber, 2002; Wang et al., 2002). In this regard, Fraldi et al. (2019) recently proved the necessity of removing the hypothesis of rigid struts in tensegrity structures (Coughlin and Stamenović, 1997), when used to characterize cells structural mechanisms as deformable systems for storing/releasing energy subjected to pre-stress changes and buckling-driven configurational switching.

Recently, drawing inspiration from the aforementioned mechanical model by Cao et al. (2015, 2017), Palumbo et al. (2022) have proposed a nonlinear elastic tensegrity model of an adherent cell to investigate the role played by actomyosin contractility of stress fibers in nucleation, growth and disassembling of focal adhesions. The model consists of a tensegrity system formed by an actomyosin stress-fiber system in parallel with a microtubule and linked to springs simulating the complex of the focal adhesions and the substrate and the nucleus. Neo-Hookean stress–strain laws are adopted for the system components, while the stiffness of the ensemble built from the ECM and the focal adhesion complex as well as the nucleus stiffness are modeled as linear springs. The outcomes have provided a new kinematical interpretation of cellular contractile forces deriving from the mechanobiological interaction of stress fibers, microtubules and focal adhesion plaques.

Upon the same premises set by Palumbo et al. (2022), in the present contribution, we consider both pre-contraction of the actomyosin and pre-polymerization of the microtubules in full recognition of their relevant role in cell stability and focal adhesion assembly. Furthermore, the assembly and disassembly of the focal adhesion plaque is studied by extending the hypothesis of nonlinear, Neo-Hookean material to the plaque itself, a novel upgrade that allows to remove the restriction of infinitesimal strains when computing the plaque growth rate.

The outline of the paper is hereafter briefly specified. Firstly, Section 2 synthetically recalls the physical circumstances under which microtubule buckling manifests. The remainder of the paper is structured in two parts, traceable back to Sections 3–4 and Sections 5–6, respectively. The former part deduces the analytical expressions pertaining to the system kinematics and the focal adhesion plaque growth. The latter part highlights and quantitatively discusses the relevant outcomes in terms of buckling, incremental stretches and plaque growth.

2. Biophysical framework

The state-of-the-art literature reports several evidences of the fact that microtubules can exert pushing forces on chromosomes and nucleus during their polymerization (Gudimchuk et al., 2020). Buckling against obstacles and polymerization of microtubules have been observed both in vitro ed in vivo. Particularly, acto-myosin contractility has been reported to promote microtubules buckling in motile cells in a process involving actin retrograde and anterograde flows. A thorough discussion about the role played by the microtubules on the cellular mechanisms can be found in the study by Bicek et al. (2009), and, for brevity, we refer to the references therein reported for a complete review of the most relevant contributions.

We focus on the contractile activity of the cytoskeleton regarded as an ensemble of myosin fibers, microtubules, and actin filaments. On the one hand, actin bundles develop mechanical links to the substrate by means of the integrins anchorage to the substrate through focal-adhesions structures. On the other hand, within the cell, the components form a network of structural elements resisting to tensile and compressive mechanical actions and transmitting forces to the substrate. In particular, microtubules confer shape and stability to the cell, while stress fibers allow cell motion. The emerging network is linked to the substrate by means of the focal adhesion complex as well as to the nucleus. The resulting system is sketched in Fig. 1, which shows the cytoskeleton of an adherent cell as an ensemble comprising the nucleus and the cytoskeleton compartment, including a component representative of the actomyosin stress fibers bundle, and a microtubule. The scheme includes also the focal adhesion complex, comprising the adhesion plaque and integrin receptors anchored to the extracellular matrix through the cell membrane.

The present study aims to consider a class of phenomena where it is possible to grossly recognize a two-elements-system where one element is prone to buckling, while the other one deforms remaining rectilinear. Examples are the case where the actomyosin system becomes unstable as a consequence of the buckling of microtubules induced either by polymerization (Murrell and Gardel, 2012) or by the pre-contraction of the actomyosin complex (Bicek et al., 2009). A simplified sketch of these latter circumstances is shown in Fig. 2. In the sketch, the contractile system in blue mimics either the behavior of a single actomyosin complex or, symbolically, stands for a whole bundle of actomyosin filaments. Analogously, the element in green can be regarded either as a single microtubule or as a network of microtubules prone to buckling and to sub-cellular polymerization. On the top of Fig. 2, buckling of the microtubular component is activated as a consequence of an inelastic pre-contraction of the actomyosins component, so that the model contracts and pulls the focal adhesions-ECM complex. In the bottom part, the microtubular component buckles as a result of its inelastic elongation ascribable to pre-polymerization, with the consequence that the model expands and exerts a compressive force on the focal-adhesions-ECM complex.

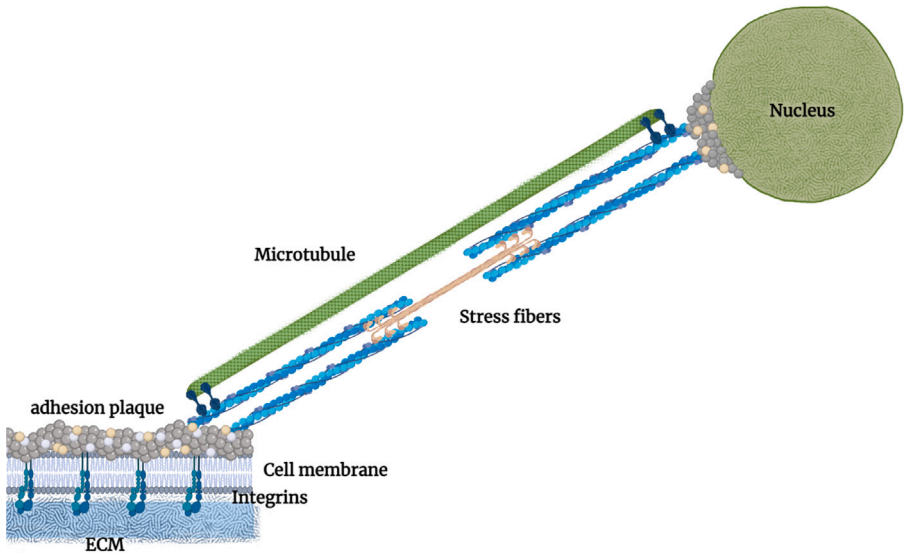

Fig. 1. Sketch of an adherent cell comprising the nucleus, the cytoskeletal compartment, made of components representative of the actomyosin stress fibers bundle and a microtubules element, and the focal adhesion complex.

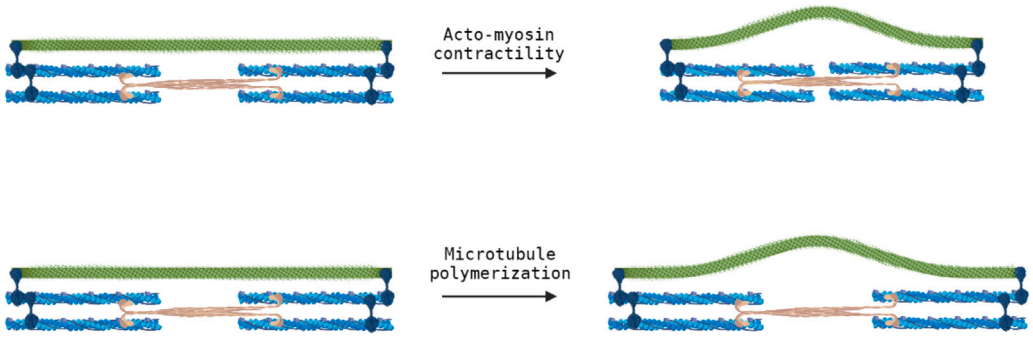

Fig. 2. Microtubule buckling. Here, the contractile system mimics either the behavior of a single actomyosin complex or symbolically stands for a whole bundle of actomyosin filaments, as well as the buckling-prone element in green can be regarded either as a single microtubule or as a network of microtubules prone to buckling and to sub-cellular polymerization.

3. Mechanical model

In light of the class of the biological phenomena that were introduced in Section 2, the cell scheme of Fig. 1 is simulated by resorting to the self-equilibrium principle of tensegrities (Palumbo et al., 2018) implemented in the model shown in Fig. 3(a). This is a mechanical system formed by an element representing the actomyosin complex, seen as a bundle of stress fibers, that can only elastically elongate or inelastically contract without bending, and a buckling-prone microtubule. The contributions ascribed to the former and the latter elements will be hereafter indicated with the pedices f and t, respectively.

The stiffnesses of the focal-adhesions–extracellular matrix complex and the nucleus are simulated by means of the springs k_{eff} and k_n, respectively. A rotational spring with stiffness κ is introduced, and it is meant to represent the microtubule bending stiffness. We idealize the pulling force exerted by the actomyosin complex on the focal adhesions-ECM system as two forces F_a acting immediately before and after the mechanical system.

The sequence of the considered configurations is displayed in Fig. 3(a). It includes the initial and the final states. In particular, L_f and L_t are the initial half lengths of the fibers system and microtubule. Application of the pre-stretches λ_f^* and λ_t^* to the fibers bundle and microtubule leads to a straight intermediate configuration, starting from which, upon reaching a critical pre-strain value, the microtubule may buckle. Finally, the ultimate configuration is characterized by the semi-lengths of the components ℓ_f and ℓ_t, resulting from further incremental stretches, hereafter indicated with $\hat{\lambda}_f$ and $\hat{\lambda}_t$.

After a premise about the equivalent stiffness of the focal adhesions-ECM complex in Section 3.1, in Section 3.2, we analytically assess the equilibrium configurations coexisting with buckled microtubules.

3.1. Stiffness of the focal adhesions-ECM complex

The stiffness of the focal-adhesion-ECM complex and the nucleus are modeled as linear springs of stiffness k_{eff} and k_n, respectively. The expression of the effective stiffness constant k_{eff} is

$$k_{eff} = \frac{d_i(k_p + k_s)}{L_c}\left[\frac{L_p}{L_c} + 2\,\mathrm{csch}\frac{L_p}{L_c} + \left(\frac{k_p}{k_s} + \frac{k_s}{k_p}\right)\coth\frac{L_p}{L_c}\right]^{-1},$$
$$L_c = d_i\sqrt{\frac{k_p k_s}{k_i(k_p + k_s)}} \tag{1}$$

and was derived by Cao et al. (2015). In Eq. (1), the value of k_{eff} depends both on geometrical features, such as the length of the adhesion plaque L_p and the average spacing d_i between integrins, and on the mechanical properties of the single constituents, more precisely, the stiffness k_i of the integrins and the stiffnesses $k_p = E_p A_p/d_i$ and $k_s = E_s A_s/d_i$ characterizing the adhesion plaque and the ECM/substrate, respectively. Here, E_p and E_s indicate the corresponding Young moduli and A_p and A_s the nominal cross-sectional areas. The associated profile

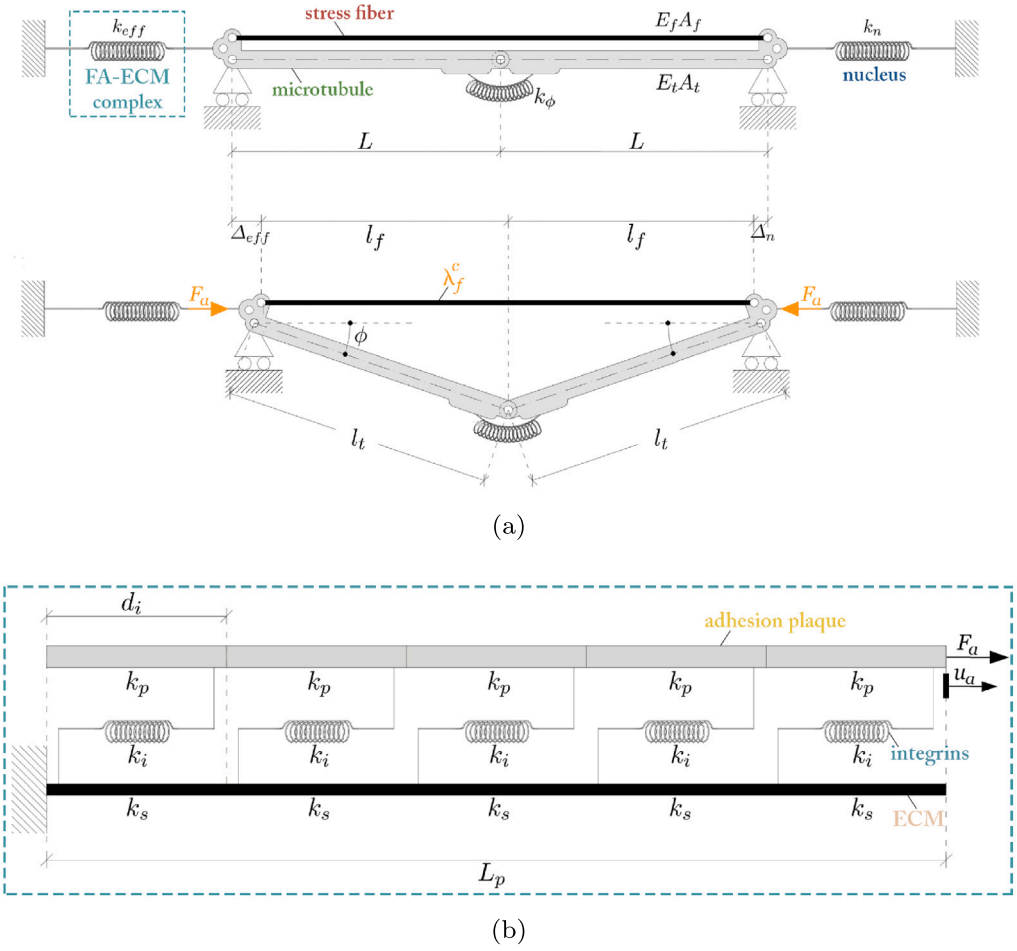

Fig. 3. (a) Mechanical model of the adherent cell in its stress-free reference state and in its current deformed configuration, with possible buckling of the microtubular element, as a consequence of the actomyosin contraction or microtubules polymerization; (b) Sketch of the structural scheme adopted for the focal adhesions–extracellular matrix complex having overall equivalent stiffness k_{eff}.

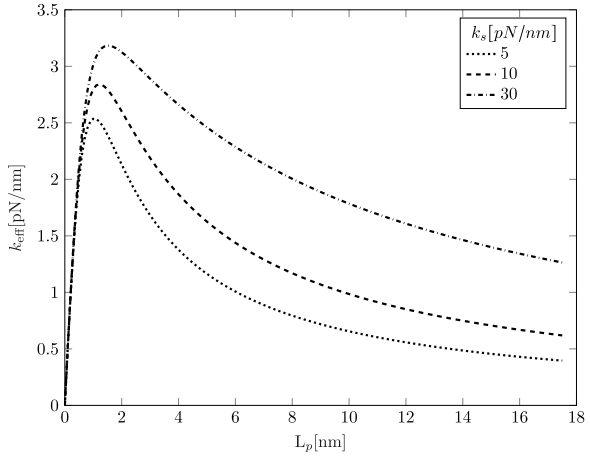

Fig. 4. The effective stiffness of a focal adhesion k_{eff} as a function of its size and ECM stiffness K_s.

of k_{eff} is shown in Fig. 4 as a function of the focal adhesion plaque length for different values of ECM stiffness. It can be drawn that the dependence of k_{eff} on L_p/d_i is not monotone as it increases up to a limit value, there reaches a peak and subsequently decreases.

3.2. Contractility and buckling activated via pre-contraction and/or pre-polymerization

For generality, we allow the microtubule and the fibers bundle to be pre-stretched with different pre-stretches λ_t^* and λ_f^*, pre-stretching being possibly induced by growth-induced polymerization/de-polymerization of the segments, as well as by a contraction of the fibers bundle. The polymerization or the contraction pre-stretches, therefore, will induce further incremental stretches $\hat{\lambda}_t$ and $\hat{\lambda}_f$, respectively. Therefore, as for the structural scheme here adopted, the stress fibers bundle is subjected to the longitudinal stretch λ_f

$$\lambda_f = \lambda_f^* \hat{\lambda}_f, \tag{2}$$

obtained through multiplicative superposition of the inelastic contractile stretch $\lambda_f^* \in]0,1]$ and the elastic incremental contribution $\hat{\lambda}_f \in [1,+\infty[$. Therefore, the current length of the fibers bundle is

$$2\ell_f = 2L_f\lambda_f = 2L_f\lambda_f^*\hat{\lambda}_f, \tag{3}$$

where $L_f = L$ identifies the rest half-length of the fiber.

By analogy, the microtubule exhibits a longitudinal stretch λ_t obtained via multiplicative superposition of the inelastic stretch $\lambda_t^* \in [1,+\infty[$ due to polymerization, and the elastic contribution $\hat{\lambda}_t \in]0,1]$:

$$\lambda_t = \lambda_t^* \hat{\lambda}_t. \tag{4}$$

As a consequence, the current length of the microtubule can be expressed as:

$$2\ell_t = 2L_t\lambda_t = 2L_t\lambda_t^*\hat{\lambda}_t, \tag{5}$$

where $L_t = L$ identifies the rest half-length of the microtubule. Moreover, the actual state of the microtubule is defined by its inclination angle $\phi \in [0, \pi/2[$ depending on whether the microtubules are buckled or not, due to high levels of contraction in the stress fibers or to excessive polymerization in the microtubule.

By making reference to a general actual configuration of the overall system with buckled microtubular component similar to that shown in Fig. 3(a), by geometrical compatibility, the fibers semi-lengths obey the following relation

$$\ell_f = \ell_t \cos\phi, \tag{6}$$

which, by virtue of Eqs. (3) and (5), leads to write

$$\hat{\lambda}_f = \frac{\lambda_t^*\hat{\lambda}_t\cos\phi}{\lambda_f^*}. \tag{7}$$

Furthermore, compatibility also prescribes that:

$$\Delta = \Delta_{eff} + \Delta_n = 2(L - \ell_f) = 2L(1 - \lambda_f^*\hat{\lambda}_f) = 2L(1 - \lambda_t^*\hat{\lambda}_t\cos\phi), \tag{8}$$

where

$$\Delta_{eff} = \alpha\Delta, \qquad \Delta_n = (1-\alpha)\Delta, \tag{9}$$

with $\alpha \in [0, 1]$, are the displacements of the focal adhesions-ECM complex and the side of the nucleus, respectively.

Both microtubule and fibers obey an incompressible Neo-Hookean law. Therefore, the hyper-elastic energies $\mathcal{U}_t$ and $\mathcal{U}_f$ stored by each of the half-lengths of the fibers bundle and the microtubule are

$$\mathcal{U}_t = \frac{K_t L_t \lambda_t^*}{6}\left[\hat{\lambda}_t^2 + \frac{2}{\hat{\lambda}_t} - 3\right], \tag{10a}$$

$$\mathcal{U}_f = \frac{K_f L_f \lambda_f^*}{6}\left[\hat{\lambda}_f^2 + \frac{2}{\hat{\lambda}_f} - 3\right] = \frac{K_f L_f \lambda_f^*}{6}\left[\left(\frac{\lambda_t^*\hat{\lambda}_t\cos\phi}{\lambda_f^*}\right)^2 + \frac{2\lambda_f^*}{\lambda_t^*\hat{\lambda}_t\cos\phi} - 3\right], \tag{10b}$$

where $K_t = E_t A_t$ and $K_f = E_f A_f$ are the related axial stiffnesses, with E_t and E_f representing the Young moduli and A_t and A_f the cross-sectional areas.

To account for large angle variations $\Delta\phi$ of the rotational spring at the middle of the microtubular component, with $\Delta\phi = 2\phi$, a nonlinear rotational spring is assumed. Its elastic energy is taken in the form (Palumbo et al., 2022):

$$\mathcal{U}_s = -2\kappa \ln\left|\cos\frac{\Delta\phi}{2}\right|. \tag{11}$$

Thus, the moment exerted from the spring is

$$M_s = \kappa \tan\frac{\Delta\phi}{2}, \tag{12}$$

where $\kappa = \pi^2 B_t/L$ is the rotational stiffness constant, B_t being the microtubule bending stiffness. Moreover, the energies $\mathcal{U}_{eff}$ and $\mathcal{U}_n$ of the focal adhesions-ECM complex and the nucleus, respectively, are written as:

$$\mathcal{U}_{eff} = \frac{1}{2}k_{eff}\,\Delta_{eff}^2 = 2k_{eff}\,\alpha^2 L^2(1 - \lambda_t^*\hat{\lambda}_t\cos\phi)^2, \tag{13a}$$

$$\mathcal{U}_n = \frac{1}{2}k_n\Delta_n^2 = 2k_n(1-\alpha)^2 L^2(1 - \lambda_t^*\hat{\lambda}_t\cos\phi)^2. \tag{13b}$$

By virtue of the aforementioned assumptions, the total potential energy of the developed mechanical system takes the form:

$$\mathcal{P}(\alpha, \hat{\lambda}_t, \phi) = 2(\mathcal{U}_t + \mathcal{U}_f) + \mathcal{U}_{eff} + \mathcal{U}_n + \mathcal{U}_s. \tag{14}$$

The equilibrium equations can be then obtained by imposing stationary conditions for $\mathcal{P}$ with respect to the Lagrangian parameters of the structure.

$$\frac{\partial\mathcal{P}}{\partial\alpha} = \frac{\partial\mathcal{P}}{\partial\phi} = \frac{\partial\mathcal{P}}{\partial\hat{\lambda}_t} = 0. \tag{15}$$

After some algebraic manipulations, the stationary conditions (15) lead to the following system of equations:

$$\alpha k_{eff} - (1-\alpha)k_n = 0, \tag{16a}$$

$$\sin\phi\left\{ b\left[\frac{(\lambda_f^*)^2}{\lambda_t^*\hat{\lambda}_t\cos^2\phi} - \frac{(\lambda_t^*)^2\hat{\lambda}_t^2\cos\phi}{\lambda_f^*}\right] + \frac{2\kappa}{\cos\phi} + 4L^2A_k\lambda_t^*\hat{\lambda}_t(1 - \lambda_t^*\hat{\lambda}_t\cos\phi)\right\} = 0, \tag{16b}$$

$$\left\{a\lambda_t^* + \left[\frac{b}{\lambda_f^*} + 4L^2A_k\right](\lambda_t^*)^2\cos^2\phi\right\}\hat{\lambda}_t^3 - 4L^2A_k\lambda_t^*\cos\phi\,\hat{\lambda}_t^2 - a\lambda_t^* - \frac{b(\lambda_f^*)^2}{\lambda_t^*\cos\phi} = 0, \tag{16c}$$

where the settings

$$a := \frac{2K_tL_t}{3}, \qquad b := \frac{2K_fL_f}{3}, \qquad A_k := k_{eff}\,\alpha^2 + k_n(1-\alpha)^2 \tag{17a}$$

have been cast. It is straightforward to recognize that Eq. (16a) holds for non trivial Δ if

$$\alpha = \frac{k_n}{k_{eff} + k_n}. \tag{18}$$

Solution of Eq. (16b) is instead given either by the trivial condition $\phi = 0$, which provides the intermediate straight state of the cell system in which the microtubule only deforms axially, or by the solution of the following equation:

$$b\left[\frac{(\lambda_f^*)^2}{\lambda_t^*\hat{\lambda}_t\cos^2\phi} - \frac{(\lambda_t^*)^2\hat{\lambda}_t^2\cos\phi}{\lambda_f^*}\right] + \frac{2\kappa}{\cos\phi} + 4L^2A_k\lambda_t^*\hat{\lambda}_t(1 - \lambda_t^*\hat{\lambda}_t\cos\phi) = 0, \tag{19}$$

which identifies the buckled configurations (i.e. $\phi \neq 0$) occurring when the compressive force withstood by the microtubule overcomes a critical threshold as an effect of the actomyosin contraction or of the microtubule polymerization. By then replacing $\cos\phi = (\lambda_f^*\hat{\lambda}_f)/(\lambda_t^*\hat{\lambda}_t)$, after some algebraic manipulations, Eqs. (19) and (16c) can be respectively recast as:

$$(b + 4L^2A_k\lambda_f^*)\hat{\lambda}_f^3 - 4L^2A_k\hat{\lambda}_f^2 - \frac{2\kappa}{\lambda_f^*}\hat{\lambda}_f - b = 0, \tag{20a}$$

$$\hat{\lambda}_t^3 + \frac{\lambda_f^*}{a\lambda_t^*\hat{\lambda}_f}\left\{4L^2A_k\hat{\lambda}_f^2(\lambda_f^*\hat{\lambda}_f - 1) + b\left[\hat{\lambda}_f^3 - 1\right]\right\}\hat{\lambda}_t - 1 = 0. \tag{20b}$$

Then, resolution of the cubic Eq. (20a) with respect to the unknown $\hat{\lambda}_f$, by resorting to Cardano's formula, provides

$$\hat{\lambda}_f = -\frac{a_2}{3a_3} + \sqrt[3]{-\frac{q_f}{2} + \sqrt{D_f}} + \sqrt[3]{-\frac{q_f}{2} - \sqrt{D_f}}, \tag{21}$$

where

$$D_f = \frac{q_f^2}{4} + \frac{p_f^3}{27}, \qquad p_f = \frac{a_1}{a_3} - \frac{a_2^2}{3a_3^2}, \qquad q_f = \frac{a_0}{a_3} - \frac{a_1a_2}{3a_3^2} + \frac{2a_2^3}{27a_3^3},$$

$$a_3 = b + 4L^2A_k\lambda_f^*, \qquad a_2 = -4L^2A_k, \qquad a_1 = -\frac{2\kappa}{\lambda_f^*}, \qquad a_0 = -b.$$

From Eq. (20b), we obtain a cubic equation with respect to the unknown $\hat{\lambda}_t$. By exploiting Cardano's formula once again, the solution turns out being expressed as

$$\hat{\lambda}_t = \sqrt[3]{-\frac{q_t}{2} + \sqrt{D_t}} + \sqrt[3]{-\frac{q_t}{2} - \sqrt{D_t}}, \tag{22}$$

where

$$D_t = \frac{q_t^2}{4} + \frac{p_t^3}{27},$$
$$p_t = \frac{\lambda_f^*}{a\lambda_t^*\hat{\lambda}_f}\left\{4L^2 A_k \hat{\lambda}_f^2(\lambda_f^*\hat{\lambda}_f - 1) + b\left[\hat{\lambda}_f^3 - 1\right]\right\}, \qquad q_t = -1.$$

Having obtained both $\hat{\lambda}_t$ and $\hat{\lambda}_f$, Eqs. (7) and (8) make it possible to compute the angle ϕ and the displacement Δ in the post-buckling phase as

$$\phi = \arccos\frac{\lambda_f^*\hat{\lambda}_f}{\lambda_t^*\hat{\lambda}_t}, \qquad \Delta = 2L(1 - \hat{\lambda}_f\lambda_f^*), \tag{23}$$

the bifurcation condition hence reading as

$$\lambda_f^*\hat{\lambda}_f = \lambda_t^*\hat{\lambda}_t. \tag{24}$$

From Eq. (24), one can deduce either the critical value of the contractile stretch λ_f^* as a function of the microtubule polymerization stretch or, *vice versa*, the critical polymerization level λ_t^* triggering the buckling event once assigned the degree of actomyosin contraction.

Finally, the mechanical force acting on the focal adhesions-ECM complex can be readily computed as

$$F_a = k_{eff}\,\Delta_{eff} = k_{eff}\,\alpha 2L(1 - \hat{\lambda}_f\lambda_f^*). \tag{25}$$

The relevant kinematics will be validated in Section 5 for variable values of the pre-stretches.

4. Mechano-chemical control of the growth rate of focal adhesions

In the present section, we derive the law governing the growth of the focal adhesion plaque in terms of the mechanical force exerted by the developed mechanical model. We purposely draw inspiration from the seminal study about kinetics and energetics of linear polymerizing systems by Hill and Kirschner (1982), where the issue of computing actin filaments assembly and disassembly was treated by analogy with the problem of a polymer under a moveable force of either thermodynamical or mechanical origin. In this seminal paper, a quadratic contribution in terms of the mechanical force appears in the expression of the growth function as a direct consequence of assuming linear elasticity. Nevertheless, this quadratic contribution has been often neglected with the motivation that it was less influential, thus restricting the growth rate of the focal adhesion plaque to be a purely linear function of the mechanical force acting on it. In particular, linear elasticity was assumed, for instance, by Shemesh et al. (2005) and Cao et al. (2015) as well as in the recent authors' contribution (Palumbo et al., 2022). This hypothesis is removed in the present study to take full account of the fact that nonlinear elasticity of Neo-Hookean type may be more appropriate to describe the overall behavior of the focal adhesion plaque, hereafter called, for brevity, plaque.

Let λ_p and F_p denote the stretch of the plaque and the force exerted by the system on the plaque, respectively, while E_p and A_p are the Young modulus and cross section of the plaque, respectively.

Following Hill (1981), Hill and Kirschner (1982), we assume a chemical potential μ_p for the plaque, and consider that, in virtue of the thermodynamical laws, an infinitesimal variation of the force acting on the plaque, F_p, induces an infinitesimal variation $d\mu_p$ as follows

$$d\mu_p = -l_m(F_p)dF_p = -\lambda_p(F_p)d_i dF_p, \tag{26}$$

where $l_m(F) = \lambda_p(F_p)d_i$ is the actual length of the single molecular constituent and d_i is the molecular length of each monomer. Assuming a Neo-Hookean behavior, the plaque stretch is

$$\lambda_p = \frac{F_p^2}{\beta_p\alpha_p} + \frac{F_p}{\alpha_p} + \frac{\beta_p}{\alpha_p}, \tag{27}$$

where $\alpha_p = E_pA_p$ and $\beta_p = 2^{-1/3}\left[\alpha_p^3 + 2F_p^3 + (\alpha_p^6 + 4\alpha_p^3F_p^3)^{1/2}\right]^{1/3}$ (Santos and Almeida Paulo, 2011; Palumbo et al., 2018). As will be better specified in Section 6.2, a numerical solution is sought by approximating λ_p with its expansion $\tilde{\lambda}_p$ in Taylor series in terms of F_p in the neighborhood of the bifurcation load. Finally, the chemical potential at the reference position coordinate X is computed by integration of Eq. (26) as:

$$\mu_p(X) = \mu_p^0 - d_i\int_0^{F_p(X)}\tilde{\lambda}_p(f_p)df_p, \tag{28}$$

where μ_p^0 is the chemical potential characterizing the plaque subunit in absence of mechanical forces. The difference between the chemical potentials $\mu_p(X)$ and μ_{free} associated with the bounded and the free molecules, respectively, is cast as:

$$\Delta\mu(X) = \mu_p(X) - \mu_{free} = \mu_p^0 - d_i\int_0^{F_p(X)}\tilde{\lambda}_p(f_p)df_p - \mu_{free}$$
$$= \Delta\mu_0 - d_i\int_0^{F_p(X)}\tilde{\lambda}_p(f_p)df_p, \tag{29}$$

$\Delta\mu_0 = \mu_p^0 - \mu_{free}$ being the chemical potential variation at vanishing force.

In the overall kinematics, $\Delta\mu$ plays, therefore, the role of driving force for the transfer of monomers between the plaque and the surroundings, in such a way that non-assembled molecules will tend to join the plaque if $\Delta\mu < 0$ and leave the plaque if $\Delta\mu > 0$. Assuming the local molecular flux towards the plaque $j(X) = -D\Delta\mu(X)$, with D a positive coefficient governing the assembly kinetics, and considering that the exchange of molecules essentially takes place at the sole extremities, the total growth rate of the adhesion plaque can be obtained as:

$$J = j(0) + j(L_p) = -D[\Delta\mu(0) + \Delta\mu(L_p)]. \tag{30}$$

Once again, it should be recalled that a positive and a negative flux J correspond to the assembly and disassembly of the monomers, respectively. Then, by taking into account that the plaque is free at the left end, i.e. $F_p(0) = 0$, and loaded on the right side by the axial force coming from the mechanical system, say $F_p(L_p) = F_a$, we obtain that:

$$J = -D\left[2\Delta\mu_0 - d_i\int_0^{F_a}\tilde{\lambda}_p(f_p)df_p\right]. \tag{31}$$

5. Validation of the kinematics triggered by pre-contraction and pre-polymerization

The results hereafter reported have been obtained by adopting the parameters in Table 1. The latter parameters correspond to taking a bundle of actomyosin filaments, hence the relatively large cross sectional area, and a single microtubule.

While the case of sole pre-contraction has been already discussed by Palumbo et al. (2022), the adoption of a combined state resulting from simultaneous pre-polymerization of the buckling-prone component and pre-contraction of the actomyosin component is assessed in Sections 5.1 and 5.2 for the first time.

5.1. Effects of independently applied pre-contraction and pre-polymerization

The previously obtained solution leads either to the trivial solution $\phi = 0$, corresponding to the straight configuration, or to non-vanishing values of ϕ expressed by Eq. (23), corresponding to the buckled state of the microtubule component. Since the possible buckled configurations of the microtubule component turn out being functions of the pre-stretches and the stiffness of the focal adhesions-ECM complex, we first validate the results against the variations of λ_t^*, λ_f^*, and L_p/d_i.

For the sake of comparison, we also report the effects of the sole actomyosin bundle pre-contraction obtained with $\lambda_t^* = 1$ and λ_f^* variable in the interval $[0.2, 1]$. In case of sole microtubule pre-polymerization, $\lambda_f^* = 1$ and $\lambda_t^* \in [1, 5]$ have been set. Figs. 5(a) and 5(b) show the buckling angle ϕ versus the inelastic pre-contraction λ_f^* and the pre-polymerization stretch λ_t^*, respectively. The curves refer to three different values of normalized plaque length L_p/d_i. The trends of the

Table 1
Values employed for the geometrical and constitutive parameters of the cell equivalent structural scheme and their realistic ranges.

Parameter	Description	Value	Source	Typical Value
L	MT and SF rest length	20 μm	Fraldi et al. (2019)	10–50 μm
L_p	adhesion plaque rest length	variable	Cao et al. (2015)	up to few μm
h_p	plaque height	100 nm	Franz and Müller (2005)	50–100 nm
w_n	plaque width	1000 nm	Franz and Müller (2005)	1000 nm
d_i	integrin spacing	100 nm	Cavalcanti-Adam et al. (2006)	100 nm
A_t	MT rest cross-sectional area	190 nm^2	Deguchi et al. (2006) Kurachi et al. (1995)	190 nm^2
A_f	SF rest cross-sectional area	$10^4\pi$ nm^2	Deguchi et al. (2006)	$10^4\pi$ nm^2
E_t	MT Young modulus	1.2 GPa	Fraldi et al. (2019)	1.2 GPa
E_f	SF Young modulus	1.45 MPa	Deguchi et al. (2006)	1.45 MPa
k_i	integrin stiffness	5 pN/nm	Fisher et al. (1999)	5 pN/nm
k_p	plaque stiffness	2.5 pN/nm	Banerjee and Marchetti (2012)	2.5 pN/nm
k_n	nucleus stiffness	20 pN/nm	Mathur et al. (2007) Caille et al. (2002)	10–50 pN/nm
k_s	ECM/substrate stiffness	10 pN/nm	Gentleman et al. (2003) Keene et al. (1987) Matthews et al. (2002)	10–100 pN/nm
$\Delta\mu_0$	energy barrier for protein recruitment without mechanical load	250 k_BT	Nicolas et al. (2004)	10 k_BT–250 k_BT
B_t	MT bending stiffness	215 nN μm^2	Brangwynne et al. (2006)	0.0215–215 nN μm^2

critical pre-stretches $\lambda^*_{f,cr}$ and $\lambda^*_{t,cr}$ at which the switch from straight to buckled configurations is possible are illustrated in Figs. 6(a) and 6(b) in terms of L_p/d_i. The non-trivial solution arises only for values of the inelastic pre-stretches smaller than a critical threshold $\lambda^*_{f,cr}$, in case of pre-contraction, and larger than a critical pre-elongation $\lambda^*_{t,cr}$, in case of pre-polymerization. Remarkably, $\lambda^*_{f,cr}$ and $\lambda^*_{t,cr}$ are nonlinear functions of L_p ranging in the narrow sets [0.81, 0.86] and [1.06, 1.14], respectively, though their values maintain approximately around 0.84 and 1.08, respectively, for L_p greater than $2d_i$. Figs. 7(a)–7(b) and 8(a)–8(b) describe the incremental, elastic stretches of the actomyosin component and the microtubule. These figures are specular and should be read as parts of the same plot.

Figs. 7(a) and 7(b) illustrate the elastic incremental stretches of the actomyosin fibers bundle in response to increasing levels of pre-contraction, the former, and pre-polymerization, the latter figure, for variable L_p/d_i. Analogously, Figs. 8(a) and 8(b) are dual to Figs. 7(a) and 7(b), as they show the incremental elastic stretches of the microtubule in terms of the λ^*_f and λ^*_t, respectively, obtained for the same three different values of normalized plaque length L_p/d_i. We can infer that the actomyosin component is generally more sensitive to L_p, and, thus, to the plaque stiffness, than the microtubule. Moreover, the incremental elastic stretch of each component is independent of the entity of the pre-stretch applied to the other component as soon as buckling is activated, as shown in Figs. 7(a) and 8(a). On the other hand, in the buckled configuration, the actomyosin component reacts to its pre-contraction with incremental elongations, while the microtubule responds to its pre-polymerization with an incremental contractile stretch.

5.2. Effects of combined pre-contraction and polymerization

The present section focuses on the effects of combining actomyosin fibers pre-contraction with different levels of microtubular pre-polymerization. Basically, the combination of the pre-stretches is carried out by assuming four different values of the pre-polymerization λ^*_t when $\lambda^*_f \in [0.2, 1]$, and four different values of the pre-contraction λ^*_f when $\lambda^*_t \in [1, 5]$.

Figs. 9(a)–9(b) are homologous to Figs. 5(a)–5(b) in terms of pre-polymerization combined with different pre-contraction levels, and vice versa. They show the profiles of the buckling angle ϕ in terms of the inelastic pre-stretches λ^*_f and λ^*_t, respectively, for a fixed value of the plaque length. The buckling angle ϕ increases for underlying pre-polymerization, while the microtubular component buckling due to pre-polymerization remains quite insensitive to an underlying pre-contraction. Moreover, from Fig. 9(b), we infer that the system starts directly from a deviated configuration, as a consequence of the large underlying pre-contraction levels.

The incremental stretches of the actomyosin fiber and microtubule are shown in Figs. 10(a), 10(b) and 11(a), 11(b) for a fixed value of L_p/d_i. Actually, the obtained results confirm the trends seen for the single pre-stretches cases. More precisely, during buckling, the incremental elongation of the actomyosin component increases for increasing levels of inelastic pre-contraction, while being insensitive to pre-polymerization. Analogously, during the buckling stage, the incremental stretch of the microtubule component depends on its pre-polymerization level and is almost independent of the pre-contraction levels.

Furthermore, the switch of $\hat{\lambda}_f$ from linear, for the straight configuration, to nonlinear, in the post-buckling configuration, is anticipated, and more markedly for increasing microtubule pre-polymerization levels. On the other hand, from Fig. 11(a), it can be inferred that the microtubule elastically contracts until buckling takes place. Particularly, the incremental stretch $\hat{\lambda}_t$ decreases until buckling occurs and, subsequently, keeps being constant for increasing pre-contraction levels. Noteworthy, such a constant level depends also on the microtubule pre-polymerization level, which also concurs to anticipate the switch to the buckled configuration.

6. Actomyosin contraction and microtubule polymerization as active tuners of assembly and disassembly of the focal adhesion plaque

In the present section, we give an account of the processes of assembly and disassembly obtained with the present model. According to Eq. (31), tensile forces will expectedly promote plaque assembly, whereas compressive forces will favor its disassembly (Tanaka and Kirschner, 1995; Hill, 1981; Heidemann and Buxbaum, 1994; Putnam et al., 2001; Geiger and Bershadsky, 2001). In the present model, the force F_p acting on the plaque corresponds to the force developed by the mechanical model in response to the inelastic pre-stretches λ^*_f and λ^*_t. Moreover, we also consider finite elasticity of the plaque by using a cubic expansion of the flux law. We have verified that, indeed, for the values of the forces into play, around 100 pN, and for realistic values of k_p, the Taylor expansion of the growth law is convergent already with the first three terms of the polynomial expansion. The figures reported in the present section aim to highlight the effects of increasing levels of actomyosin contraction and microtubule's polymerization on the plaque growth rate. The obtained results confirm and complete those previously obtained by the authors (Palumbo et al., 2022). In the next figures, unless specified differently, the substrate stiffness κ_s has been set equal to 10 pN/nm.

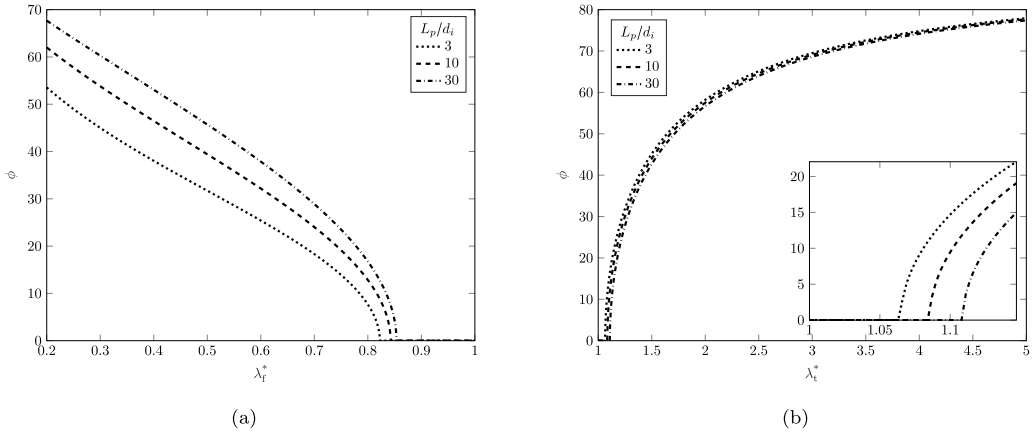

Fig. 5. Buckling angle ϕ versus the inelastic pre-contraction λ_f^* (a) and the pre-polymerization stretch λ_t^* (b), for different values of normalized plaque length L_p/d_i.

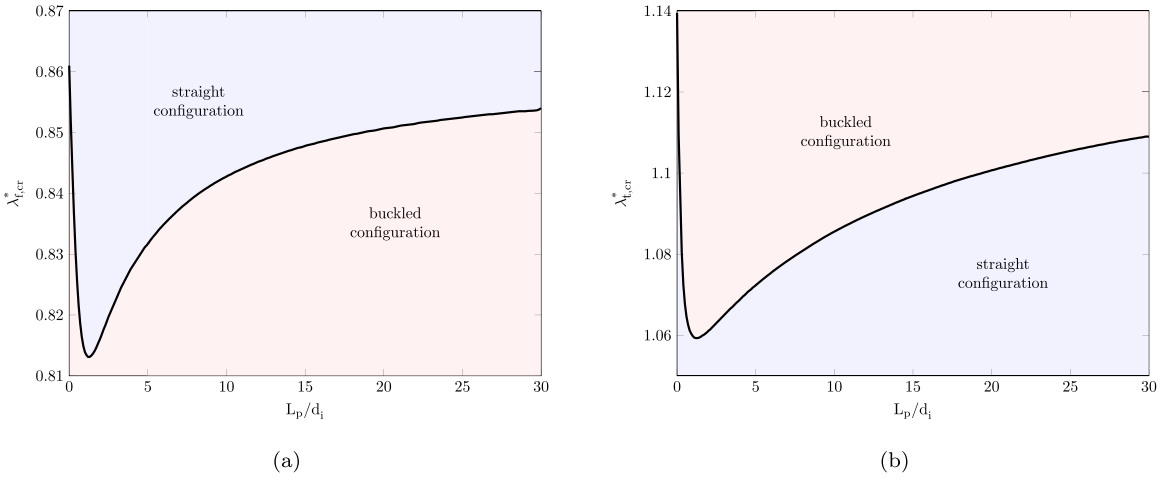

Fig. 6. Profiles of $\lambda_{f,cr}^*$ (a) and $\lambda_{t,cr}^*$ (b) as a function of the normalized plaque length L_p/d_i.

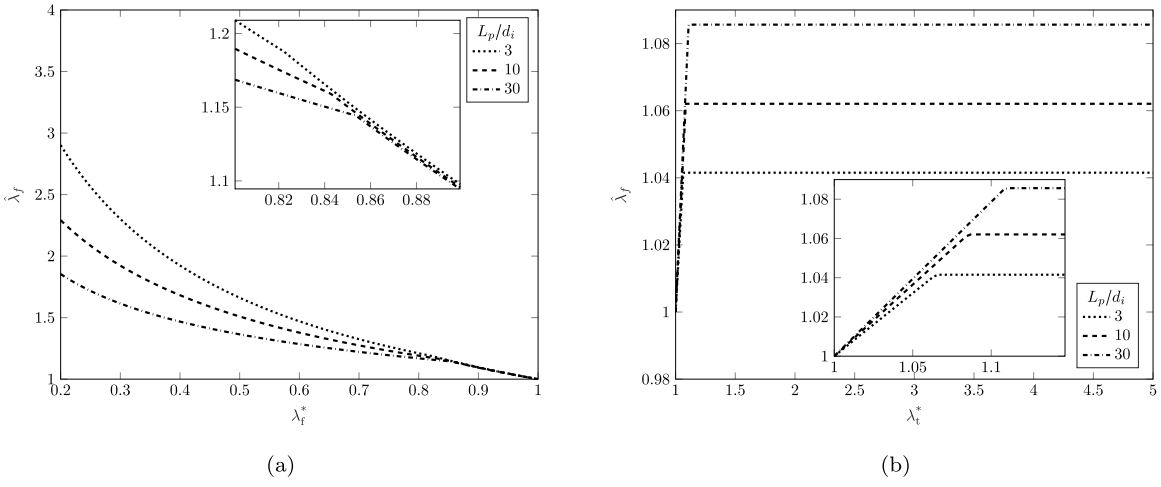

Fig. 7. Incremental elastic stretches of the actomyosin fibers bundle versus the inelastic pre-contraction stretch λ_f^* (a) and the pre-polymerization stretch λ_t^* (b). The curves refer to three different values of normalized plaque length L_p/d_i.

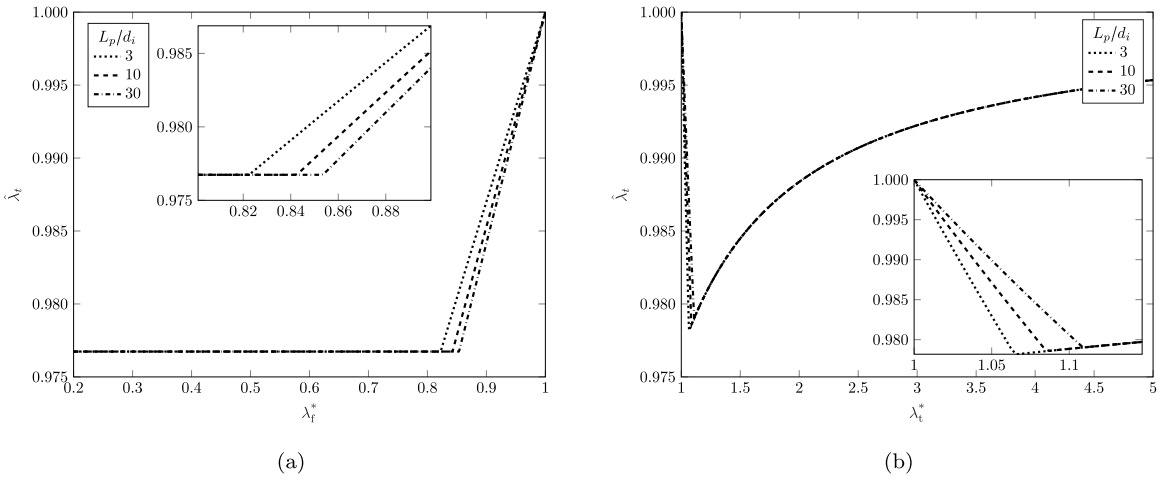

Fig. 8. Incremental elastic stretches of the microtubule versus the inelastic pre-contraction λ_f^* (a) and the pre-polymerization stretch λ_t^* (b). The curves refer to three different values of normalized plaque length L_p/d_i.

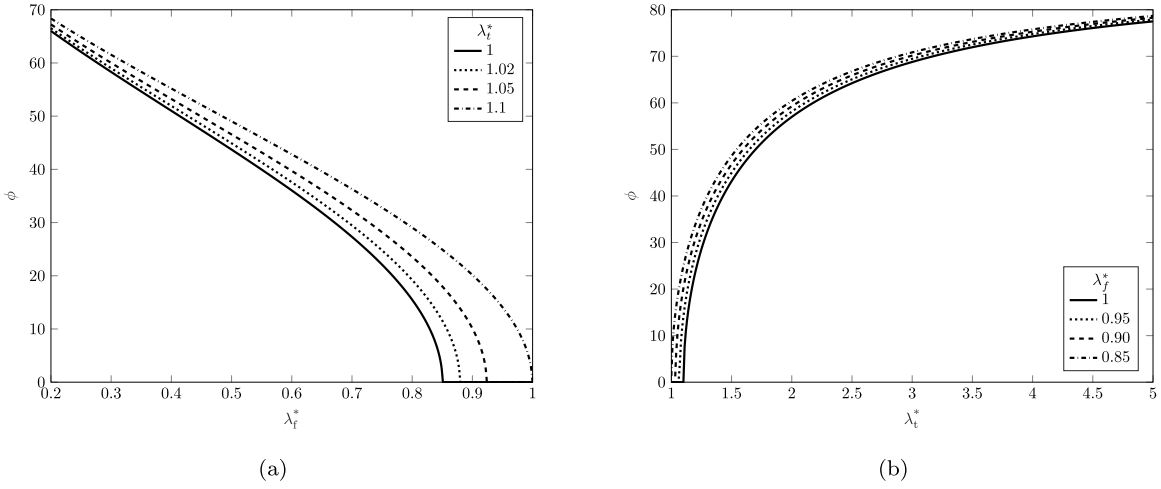

Fig. 9. Combined pre-stretches: Buckling angle ϕ plotted as a function of the pre-contraction λ_f^* for variable λ_t^* (a), and of the pre-polymerization λ_t^* for variable λ_f^* (b), setting $L_p = 20d_i$.

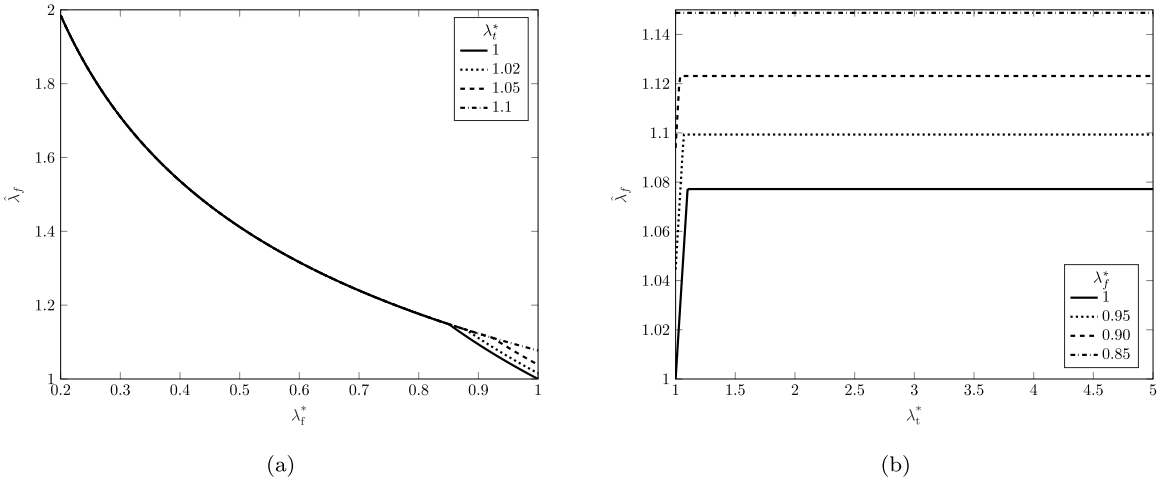

Fig. 10. Combined pre-stretches: Incremental stretches of the actomyosin bundle $\hat{\lambda}_f$ plotted as a function of the pre-contraction λ_f^* for variable λ_t^* (a) and as a function of the pre-polymerization λ_t^* for variable λ_f^* (b), setting $L_p = 20d_i$.

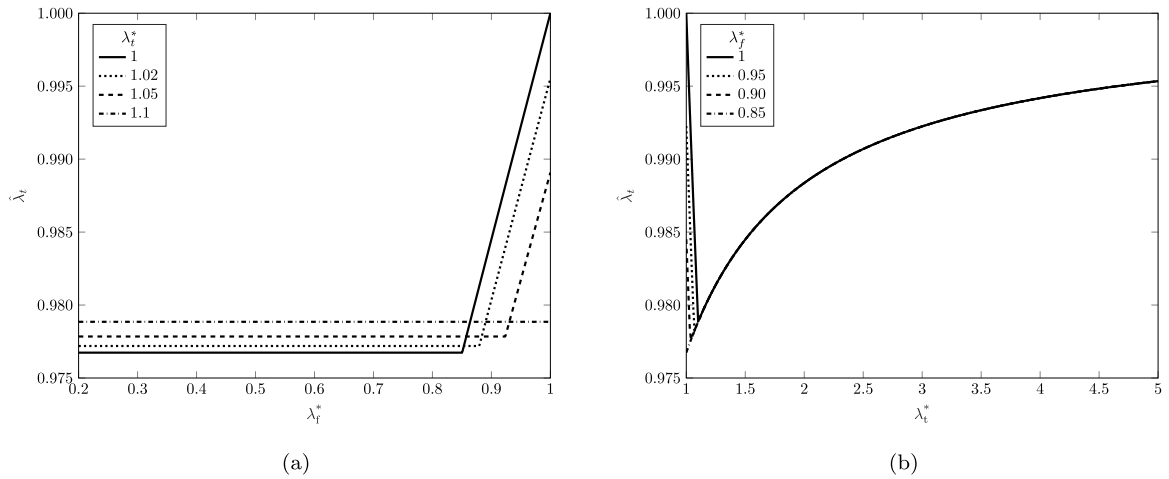

Fig. 11. Combined pre-stretches: Incremental stretches of the microtubule $\hat{\lambda}_t$ plotted as a function of the pre-contraction λ_f^* for variable λ_t^* (a) and as a function of the pre-polymerization λ_t^* for variable λ_f^*(b), setting $L_p = 20d_i$.

6.1. Combined effect of pre-contraction and polymerization on focal adhesion assembly

Worthy to be investigated, mechanosensitivity of the induced flux to pre-polymerization levels is such that their increase expectedly enhances the value of the mechanical force pushing the focal adhesions-ECM complex and, therefore, promotes the disaggregation flux of the binding proteins. We purposely investigate how actomyosin pre-contraction combined with microtubule polymerization levels influences the focal adhesion growth rate. We recall that the arising mechanical force regulates the processes of polymerization and depolymerization of the focal adhesion plaque by enhancing the negative part of flux J: the higher the compressive force pushing the plaque, the higher the plaque disaggregation.

In particular, Fig. 12(a) shows the force acting on the focal adhesions-ECM complex as a function actomyosin pre-stretches $\lambda_f^* \in [0.75, 1]$ for a fixed magnitude of the adhesion plaque $L_p = 1.4d_i$, and with four different values of the pre-stretch applied to the microtubules component λ_t^*.

It can be observed that increasing pre-contractility enhances the value of the mechanical force, all the more so in the post-buckling regime.

Fig. 12(b) shows the force pushing on the focal adhesions-ECM complex in terms of the microtubule pre-stretches, assuming $\lambda_t^* \in [1, 1.3]$ for $L_p = 1.4d_i$. Once buckling has taken place, the mechanical force remains constant, because the microtubule component cannot bear further load increases. We recall that, if the sole microtubule pre-polymerization takes place, the mechanical forces pushes on the focal adhesions-ECM complex, thus hindering plaque assembly. Moreover, it has been previously ascertained that the pre-contraction level must overcome a critical threshold to promote monomers aggregation, plaque disassembly associated with negative flux, in fact, taking place otherwise.

The mechanical force exerted on the focal adhesions-ECM complex turns out to depend on the focal adhesion length, as shown in Fig. 13(a). Furthermore, it emerges that an increase of the pre-contractility level leads to a significant increase of the value of the mechanical force pulling the focal adhesions-ECM complex, thus enhancing the flux of proteins binding to the plaque.

Fig. 13(b) describes the circumstance where pre-polymerization prevails over pre-contraction. In both Figs. 13(a) and 13(b), the profiles in blue and black correspond to buckled and straight configurations, respectively.

From the previous figures, it can be observed that an increasing contractility extent significantly concurs to increase the value of the mechanical force F_p, this effect being further amplified after the microtubule buckling occurs. Moreover, it can be inferred that positive pulling tensile forces $F_p > 0$ promote an increase of the flux J, whereas compressive forces, $F_p < 0$, tend to inhibit the assembly process and may lead to negative fluxes, $J > 0$, as shown in Figs. 14(a) and 14(b). The latter figures suggest that, indeed, three regimes of the plaque dynamics emerge (Cao et al., 2015): a nascent plaque must overcome a critical size to initiate elongation depending on the threshold $\Delta\mu^0$. If the length of the newly nucleated focal adhesion complex is lower than this critical size, the plaque will disassemble and, eventually, disappear. Beyond this critical value, a small plaque will increase its length in an effort to achieve a stable length. On the other hand, larger plaques will disassembly until they reach a stable size. This kind of behavior has been experimentally detected (Cukierman et al., 2002). Noteworthy, for increasing pre-contraction levels, the mechanical force acting on the plaque increases in such a way that the plaque continues to grow up without reaching a stable length in an unlimited assembly process. Contractility levels higher than a critical threshold are necessary to promote monomers aggregation and hamper plaque disassembly.

However, considering that, in general, the overall cell pre-strain results from different mechanisms that can be in competition with each other, the effective mechanosensitivity of the plaque will be expectedly influenced by the simultaneous presence of pre-existing deformative events at the sub-cellular level, such as pre-polymerization and pre-contraction.

Fig. 15(a) and Fig. 15(b) display the plaque force and the growth flux, respectively, plotted as a function of the adhesion plaque length L_p normalized with respect to the integrin spacing d_i for a series of values of pre-contraction combined either with no pre-polymerization ($\lambda_t^* = 1$) or with a 2‰ pre-polymerization. In fact, it has been verified that a 1‰ pre-polymerization stretch is sufficient to change the assembly process into a disassembly one, for small values of the pre-contraction. Thus, in general, it emerges that the assembly attempt of the focal adhesion plaque in response to the mechanical force induced from the cell, even on stiff substrates, might be frustrated from the competition between assembly and disassembly driving forces, while the same levels of pre-contraction could, in certain cases, promote and, in others, hamper the plaque growth.

6.2. Remarks on the growth function

This section investigates the effects inherent in the mathematical structure of the growth law. In the state-of-the-art literature, the growth function is usually expressed as a linear function of the mechanical force starting from the pioneering paper by Hill (1981) under the hypothesis of small displacements, with only few exceptions

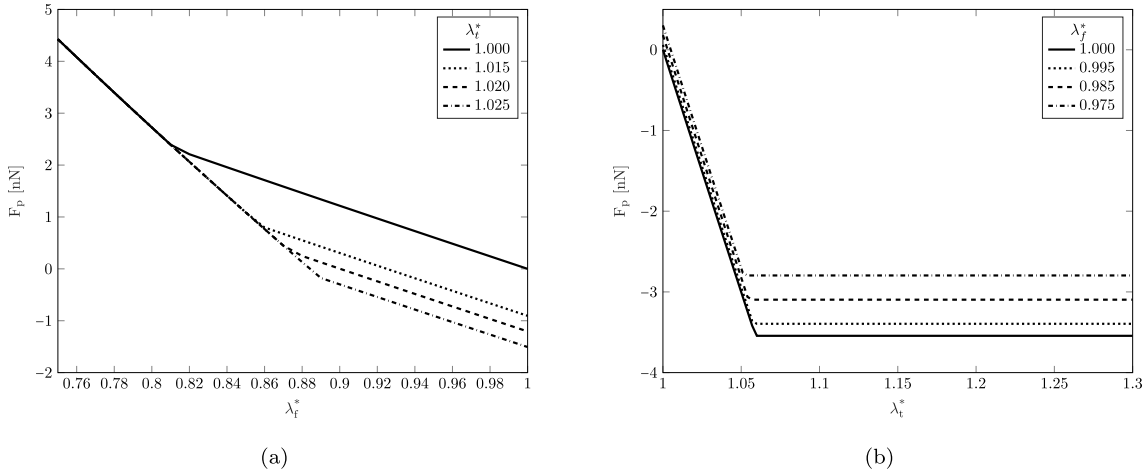

Fig. 12. Combined pre-stretches: Force F_p plotted as a function of the actomyosin bundle pre-contraction λ_f^* for four different values of the pre-polymerization stretches λ_t^* (a); Force F_p plotted as a function of the microtubule pre-polymerization λ_t^* for four different values of the pre-contraction stretches λ_f^* (b). Here, the magnitude of the adhesion plaque is $L_p = 1.4d_i$.

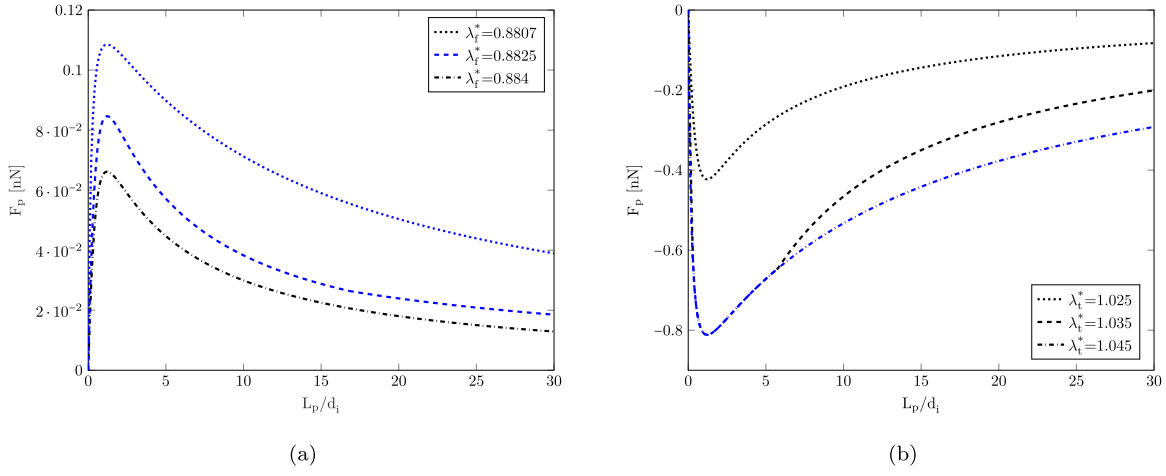

Fig. 13. Force F_p plotted as a function of L_p/d_i for the cases of pre-contraction with underlying pre-polymerization $\lambda_t^* = 1.0222$ (a) and pre-polymerization with underlying pre-contraction $\lambda_f^* = 0.91$ (b), respectively. The curves refer to three different values of inelastic pre-stretches λ_f^* and λ_t^*, respectively. The profiles in blue correspond to buckled configurations, while those in black to straight configurations.

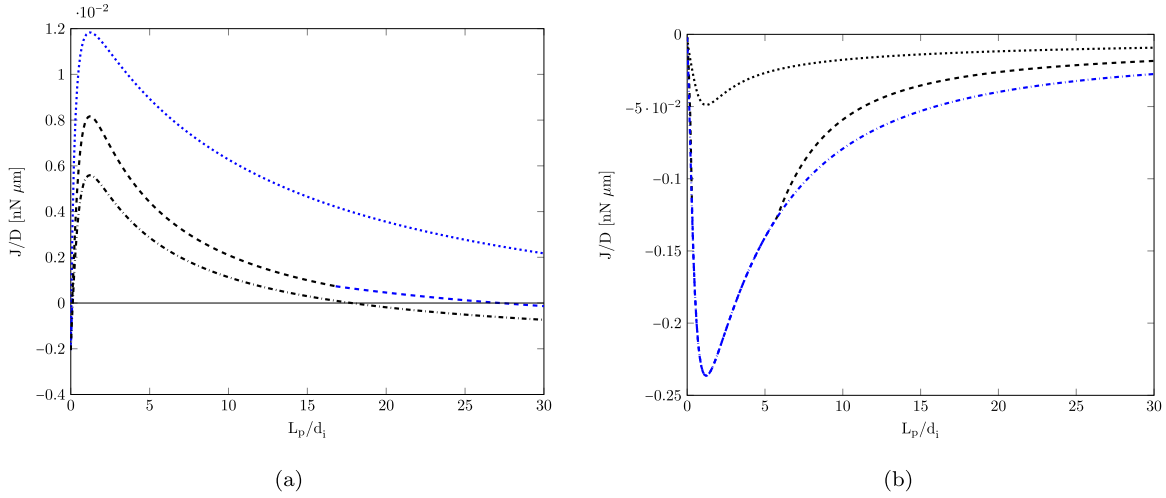

Fig. 14. Comparison between the growth law of the adhesion plaque obtained by assuming three different values of inelastic pre-contraction λ_f^* (a) and pre-polymerization λ_t^* (b). The curves have been obtained with the same values used in Figs. 13(a) and 13(b). The profiles in blue correspond to buckled configurations, while those in black to the straight configuration.

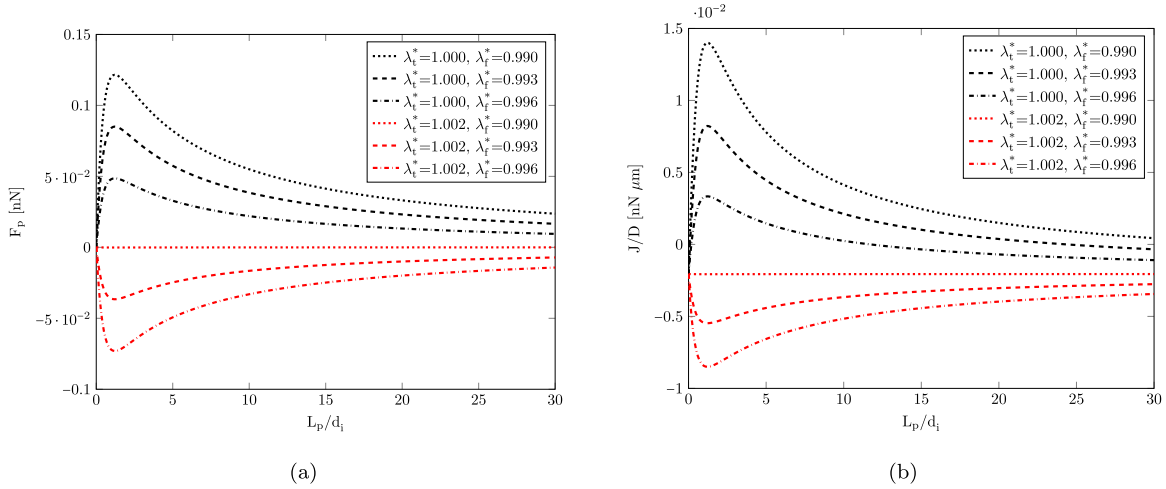

Fig. 15. Combined pre-stretches: Force F_p (a) and aggregation or disaggregation flux (b) plotted as a function of the focal adhesion plaque length L_p normalized with respect to the integrin spacing d_i.

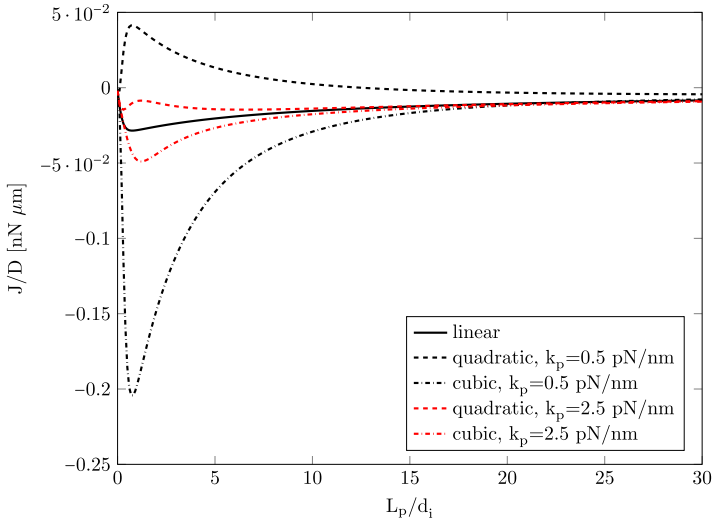

Fig. 16. Comparison between the growth law of the adhesion plaque obtained by assuming linear, quadratic and cubic form of the flux assuming two values of the plaque stiffness k_p and for a fixed pre-polymerization $\lambda_t^* = 1.025$ and $\lambda_f^* = 0.91$.

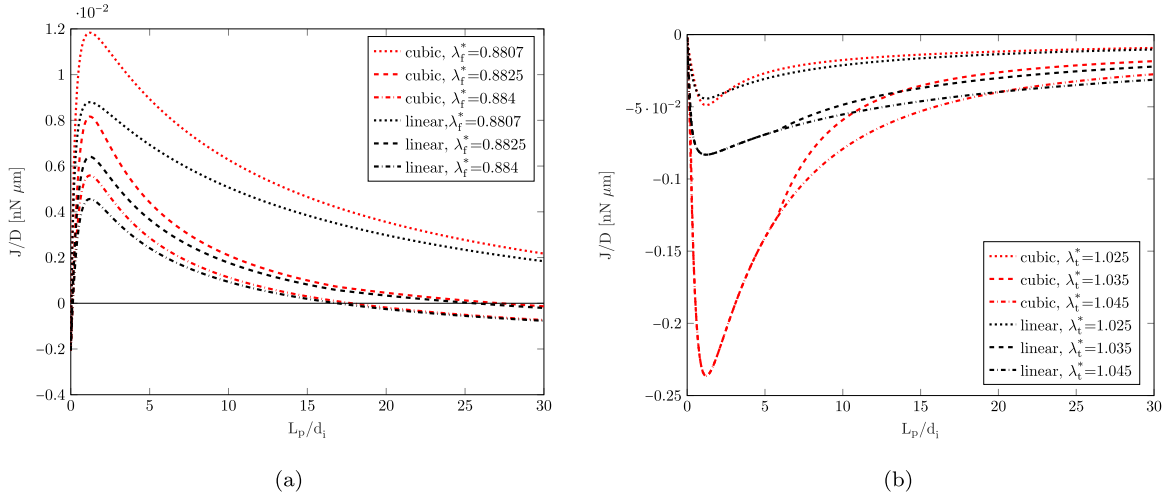

Fig. 17. Comparison between the growth law of the adhesion plaque obtained by assuming Hill and Kirschner (1982) linear law by neglecting the quadratic term (profiles in black), and the non-linear elasticity law in Eq. (31) (profiles in red), for different values of pre-contraction (a) and microtubule polymerization (b). The curves refer to three different values of inelastic pre-stretches λ_f^* and λ_t^*, respectively.

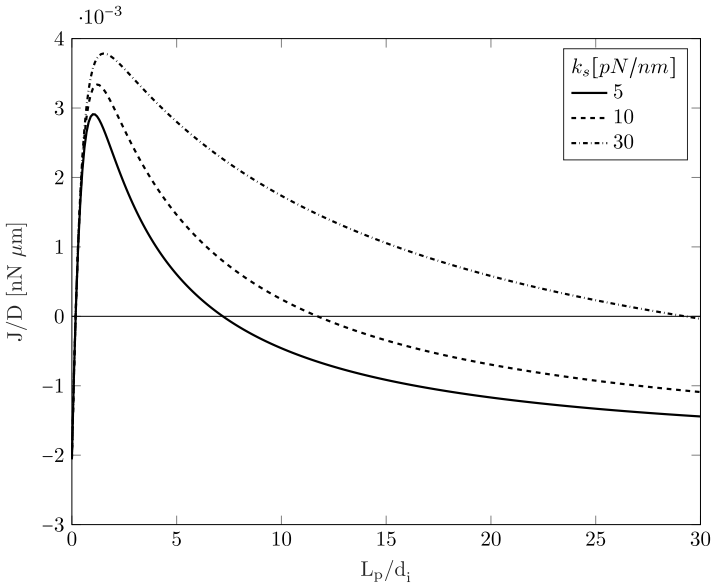

Fig. 18. Influence of the substrate stiffness on the growth flux for $\lambda_t^* = 1$ and $\lambda_f^* = 0.996$.

(Palumbo et al., 2022). However, a quantitative inconsistency appears when the quadratic term arising in the expression of the growth function J is neglected. This inconsistency occurs as soon as the mechanical force acting on the plaque is compressive, especially for values of the plaque stiffness below $\kappa_p = 1$ pN/nm, at least, for the geometrical and constitutive parameters' values considered in the present work. In fact, once fixed the other geometrical and constitutive parameters, the quadratic term can take values that become non-negligible depending on the values of κ_p, so that, in general, it seems not possible to conclude that the quadratic term can be neglected *a priori* as it is not influential. Furthermore, the quadratic term does not distinguish the sign of the force.

In this regard, Fig. 16 shows the growth laws obtained by means of linear, quadratic and cubic expressions of the growth function plotted for a 5% pre-polymerization of the microtubule component. To better clarify this aspect, Figs. 17(a) and 17(b) compare the growth laws of the focal adhesion plaque obtained by assuming both the law established in the hypothesis of small displacements (Hill and Kirschner, 1982), where, however, the quadratic term is neglected (Hill and Kirschner, 1982; Shemesh et al., 2005), profiles in black, and the cubic approximation of the growth law given in Eq. (31), profiles in red, for different values of pre-contraction (a) and microtubule pre-polymerization (b). The curves refer to three different values of inelastic pre-stretches λ_f^* and λ_t^*, respectively.

6.3. Dependence of the growth flux on the substrate stiffness

Generally, larger contractile forces are thought to develop when cells sense stiffer environments.

Fig. 18 shows that softer substrates elicit smaller stable lengths of the plaque, suggesting that the attachment of the cell is stronger and rooted over a longer plaque on stiffer substrates than on soft substrates. The obtained outcomes confirm the durotaxis phenomenon.

7. Discussion of the results

From the findings of the present research, it can be inferred that, almost independently of the plaque length, for the considered values of the involved geometrical and constitutive parameters of the cellular system, independently applied pre-stretches of pre-contraction and polymerization approximately beyond 19% and 10%, respectively, promote buckling. As soon as these pre-stretches are combined, the values of the pre-stretches that activate buckling significantly decrease, as the system buckles already with pre-stretches of the order of the 1%. On the other hand, the combination of simultaneous pre-contraction and pre-polymerization may lead to a situation where, even in the presence of significant pre-contractions, the plaque turns out being compressed by the cell, so that the assembly of the focal adhesion plaques is inhibited. For increasing pre-contraction levels, the force changes sign and focal adhesion assembly takes place. However, the critical pre-contraction at which the force inverts its sign increases for increasing pre-polymerization levels. Noteworthy, for increasing pre-contraction levels, λ_f^* below 0.88, the mechanical force acting on the plaque increases in such a way that the plaque continues to grow up without reaching a stable length in an unlimited assembly process. It is, in fact, the simultaneous presence of pre-polymerization that allows to obtain a stable length of the plaque, beyond which the assembly process stops. Assuming nonlinear elasticity of the focal adhesion plaque, increasing pre-contraction and pre-polymerization levels enhances the plaque growth flux to a greater extent than that reachable assuming linear elasticity.

7.1. Model limitations, applicability, and future perspectives

Cell locomotion is a process orchestrated by entangled chemical, mechanical and biological mechanisms, an example of which being the actin and microtubules treadmilling. It basically comes by protrusion and construction of new adhesion complexes at the leading edge, and deadhesion and contraction at the rear (Recho et al., 2013). However, in the present model, only autotaxis induced by sub-cellular contraction and polymerization is captured, whereas protrusion at the leading edge cannot be reproduced. The model, indeed, cannot confer directionality to the cell and does not allow to distinguish between trailing and leading edges.

Nevertheless, though simplified, the adopted one-dimensional framework is susceptible of being extended to supplementary aspects. Relevant examples are the influence of broken geometrical symmetry on cell stability, the connection between the forces exerted by the focal adhesion complexes and durotaxis, and the assumption of biochemically motivated nonlinear force–displacement response of the focal adhesion plaque (Deshpande et al., 2008), also accounting for frictional effects and remodeling (Di Stefano et al., 2022).

8. Conclusions

We have generalized the nonlinear tensegrity system previously devised by the authors (Palumbo et al., 2022) for the analytical investigation of the kinematics of a simplified system formed by a cytoskeleton, reduced to a nucleus and an actomyosin filaments bundle in parallel with a microtubular element, interacting with the surroundings and with the focal adhesion complexes. In the present model, buckling is triggered by pre-stretches simulating actomyosin fibers bundle contraction and microtubules polymerization, while nonlinear elasticity is considered also for the focal adhesion plaque. On the one hand, the obtained analytical expressions for the relevant kinematic fields and focal-adhesion plaque growth can be used as a tool complementary to experiments and can help devising proper experimental tests. On the other hand, the main original findings of the present research derive from having quantified and modeled the impact on the plaque growth of microtubules polymerization combined with actomyosin pre-contraction, suggesting that the effective mechanosensitivity of the plaque might be influenced by the simultaneous existence of sub-cellular polymerization and contraction. The main consequence is that the assembly response of the focal adhesion plaque to the mechanical force induced from the cell, even on stiff substrates, might be frustrated from the competition between assembly- and disassembly-driving forces, so that the same levels of pre-contraction could, in general, be associated either with assembly or disassembly of the plaque.

Noteworthy, the usefulness of the proposed tensegrity model has been proved when the contractile component corresponds to a bundle of actomyosin fibers, while the buckling-prone component is associated with a microtubule. However, upon properly setting the material parameters, it is possible to adapt the model in such a way that it captures the behavior of a single actomyosin fiber in parallel with a microtubule, or, in general, the model could be used to simulate any contractile behavior triggered by inherent buckling events.

CRediT authorship contribution statement

E. Benvenuti: Writing – review & editing, Supervision, Project administration, Methodology, Investigation, Formal analysis, Data curation, Conceptualization. **G.A. Reho:** Validation, Software, Investigation, Data curation. **S. Palumbo:** Resources, Methodology, Data curation, Conceptualization. **M. Fraldi:** Writing – review & editing, Methodology, Conceptualization.

Declaration of competing interest

The authors declare that they have no known competing financial interests or personal relationships that could have appeared to influence the work reported in this paper.

Data availability

The whole dataset was reported in the paper.

Acknowledgment

The financial support of the MIUR PRIN 2017 research project PRIN-20177TTP3S is gratefully acknowledged.

References

Banerjee, S., Marchetti, M.C., 2012. Contractile stresses in cohesive cell layers on finite-thickness substrates. Phys. Rev. Lett. 109, 108101.
Bangasser, B.L., Rosenfeld, S.S., Odde, D.J., 2013. Determinants of maximal force transmission in a motor-clutch model of cell traction in a compliant microenvironment. Biophys. J. 105 (3), 581–592.
Bershadsky, A.D., Ballestrem, C., Carramusa, L., Zilberman, Y., Gilquin, B., Khochbin, S., Alexandrova, A.Y., Verkhovsky, A.B., Shemesh, T., Kozlov, M., 2006. Assembly and mechanosensory function of focal adhesions: Experiments and models. Eur. J. Cell Biol. 85 (3), 165–173.
Bicek, A.D., Tüzel, E., Demtchouk, A., Uppalapati, M., Hancock, W.O., Kroll, D.M., Odde, D.J., 2009. Anterograde microtubule transport drives microtubule bending in LLC-PK1 epithelial cells. Mol. Biol. Cell 20 (12), 2943–2953.
Brangwynne, C.P., MacKintosh, F.C., Kumar, S., Geisse, N.A., Talbot, J., Mahadevan, L., Parker, K.K., Ingber, D.E., Weitz, D.A., 2006. Microtubules can bear enhanced compressive loads in living cells because of lateral reinforcement. J. Cell Biol. 173 (5), 733–741.
Caille, N., Olivier, T., Yanik, T., Meister, J.J., 2002. Contribution of the nucleus to the mechanical properties of endothelial cells. J. Biomech. 35 (2), 177–187.
Cao, X., Ban, E., Baker, B.M., Lin, Y., Burdick, J.A., Chen, C.S., Shenoy, V.B., 2017. Multiscale model predicts increasing focal adhesion size with decreasing stiffness in fibrous matrices. Proc. Natl. Acad. Sci. 114 (23), E4549–E4555.
Cao, X., Lin, Y., Driscoll, T.P., Franco-Barraza, J., Cukierman, E., Mauck, R.L., Shenoy, V.B., 2015. A chemomechanical model of matrix and nuclear rigidity regulation of focal adhesion size. Biophys. J. 109 (9), 1807–1817.
Cavalcanti-Adam, E.A., Micoulet, A., Blümmel, J., Auernheimer, J., Kessler, H., Spatz, J.P., 2006. Lateral spacing of integrin ligands influences cell spreading and focal adhesion assembly. Eur. J. Cell Biol. 85 (3), 219–224.
Chan, C.E., Odde, D.J., 2008. Traction dynamics of filopodia on compliant substrates. Science 322 (5908), 1687–1691.
Chrzanowska-Wodnicka, M., Burridge, K., 1996. Rho-stimulated contractility drives the formation of stress fibers and focal adhesions. J. Cell Biol. 133 (6), 1403–1415.
Coughlin, M.F., Stamenović, D., 1997. A tensegrity structure with buckling compression elements: Application to cell mechanics. J. Appl. Mech. 64 (3), 480–486.
Cowin, S.C., Doty, S.B., 2007. Tissue Mechanics. Springer.
Cukierman, E., Pankov, R., Yamada, K.M., 2002. Cell interactions with three-dimensional matrices. Curr. Opin. Cell Biol. 14 (5), 633–640.
Deguchi, S., Toshiro, O., Masaaki, S., 2006. Tensile properties of single stress fibers isolated from cultured vascular smooth muscle cells. J. Biomech. 39 (14), 2603–2610.
Deshpande, V.S., McMeeking, R.M., Evans, A.G., 2006. A bio-chemo-mechanical model for cell contractility. Proc. Natl. Acad. Sci. 103 (38), 14015–14020.
Deshpande, V.S., Mrksich, M., McMeeking, R.M., Evans, A.G., 2008. A bio-mechanical model for coupling cell contractility with focal adhesion formation. J. Mech. Phys. Solids 56 (4), 1484–1510.
Di Stefano, S., Benvenuti, E., Coscia, V., 2022. On the role of friction and remodelling in cell–matrix interactions: A continuum mechanical model. Int. J. Non-Linear Mech. 142, 103966.
Fisher, T.E., Oberhauser, A.F., Carrion-Vazquez, M., Marszalek, P.E., Fernandez, J.M., 1999. The study of protein mechanics with the atomic force microscope. Trends Biochem. Sci. 24 (10), 379–384.
Fraldi, M., Palumbo, S., Carotenuto, A.R., Cutolo, A., Deseri, L., Pugno, L., 2019. Buckling soft tensegrities: Fickle elasticity and configurational switching in living cells. J. Mech. Phys. Solids 124, 299–324.
Franz, C.M., Müller, D.J., 2005. Analyzing focal adhesion structure by atomic force microscopy. J. Cell Sci. 118 (22), 5315–5323.
Geiger, B., Bershadsky, A., 2001. Assembly and mechanosensory function of focal contacts. Curr. Opin. Cell Biol. 13 (5), 584–592.
Gentleman, E., Lay, A.N., Dickerson, D.A., Nauman, E.A., Livesay, G.A., Dee, K.C., 2003. Mechanical characterization of collagen fibers and scaffolds for tissue engineering. Biomaterials 24 (21), 3805–3813.
Gudimchuk, N.B., Ulyanov, E.V., O'Toole, E., Page, C.L., Vinogradov, D.S., Morgan, G., Li, G., Moore, J.K., Szczesna, E., Roll-Mecak, A., Ataullakhanov, F.I., McIntosh, R.J., 2020. Mechanisms of microtubule dynamics and force generation examined with computational modeling and electron cryotomography. Nature Commun. 11, 3765.
He, S., Su, Y., Ji, B., Gao, H., 2014. Some basic questions on mechanosensing in cell–substrate interaction. J. Mech. Phys. Solids 70, 116–135.
Heidemann, S.R., Buxbaum, R.E., 1994. Mechanical tension as a regulator of axonal development. Neurotoxicology 15 (1), 95—107.
Hill, T.L., 1981. Microfilament or microtubule assembly or disassembly against a force. Proc. Natl. Acad. Sci. 78 (9), 5613–5617.
Hill, T.L., Kirschner, M.W., 1982. Bioenergetics and kinetics of microtubule and actin filament assembly-disassembly. Int. Rev. Cytol. 78, 1–125.
Hirata, H., Tatsumi, H., Sokabe, M., 2008. Mechanical forces facilitate actin polymerization at focal adhesions in a zyxin-dependent manner. J. Cell Sci. 121 (17), 2795–2804.
Janmey, P.A, Fletcher, D.A., Reinhart-King, C.A., 2020. Stiffness sensing by cells. Physiol. Rev. 100 (2), 695–724.

Jansen, K.A., Donato, D.M, Balcioglu, H.E., Schmidt, T., Danen, E.H., Koenderink, G.H., 2015. A guide to mechanobiology: Where biology and physics meet. Biochim. Et Biophys. Acta (BBA) - Mol. Cell Res. 1853 (11, Part B), 3043–3052.

Kaverina, I., Krylyshkina, O., Beningo, K., Anderson, K., Wang, Y.L., Small, J.V., 2002. Tensile stress stimulates microtubule outgrowth in living cells. J. Cell Sci. 115 (11), 2283–2291.

Keene, D.R., Sakai, L.Y., Bachinger, H.P., Burgerson, R.E., 1987. Type III collagen can be present on banded collagen fibrils regardless of fibril diameter. J. Cell Biol. 105 (5), 2393–2402.

Kreis, T.E., Birchmeier, W., 1980. Stress fiber sarcomeres of fibroblasts are contractile. Cell 22 (2, Part 2), 555–561.

Kurachi, M., Hoshi, M., Tashiro, H., 1995. Buckling of a single microtubule by optical trapping forces: Direct measurement of microtubule rigidity. Cell Motil. Cytoskeleton 30 (3), 221–228.

Leijnse, N., Oddershede, L.B., Bendix, P.M., 2014. Helical buckling of actin inside filopodia generates traction. Proc. Natl. Acad. Sci..

Lo, C.M., Wang, H.B., Dembo, M., Wang, Y.L., 2000. Cell movement is guided by the rigidity of the substrate. Biophys. J. 79, 144–152.

Mathur, A.B., Reichert, W.M., Truskey, G.A., 2007. Flow and high affinity binding affect the elastic modulus of the nucleus, cell body and the stress fibers of endothelial cells.. Ann. Biomed. Eng. 35, 1120–1130.

Matthews, J.A., Wnek, G.E., Simpson, D.G., Bowlin, G.L., 2002. Electrospinning of collagen nanofibers. Biomacromolecules 3 (2), 232–238.

Murrell, M.P., Gardel, M.L., 2012. F-actin buckling coordinates contractility and severing in a biomimetic actomyosin cortex. Proc. Natl. Acad. Sci. 109 (51), 20820–20825.

Nicolas, A., Geiger, B., Safran, S.A., 2004. Cell mechanosensitivity controls the anisotropy of focal adhesions. Proc. Natl. Acad. Sci. 101 (34), 12520–12525.

Palumbo, S., Benvenuti, E., Fraldi, M., 2022. Actomyosin contractility and buckling of microtubules in nucleation, growth and disassembling of focal adhesions. Biomech. Model. Mechanobiol. 21, 1187–1200.

Palumbo, S., Carotenuto, A.R., Cutolo, A., Deseri, L., Fraldi, M., 2018. Nonlinear elasticity and buckling in the simplest soft-strut tensegrity paradigm. Int. J. Non-Linear Mech. 106, 80–88.

Putnam, A.J., Schultz, K., Mooney, D.J., 2001. Control of microtubule assembly by extracellular matrix and externally applied strain. Am. J. Physiol. Cell Physiol. 280 (3), C556–C564.

Recho, P., Putelat, T., Truskinovsky, L., 2013. Contraction-driven cell motility. Phys. Rev. Lett. 111, 108102.

Santos, H.A.F.A., Almeida Paulo, C.I., 2011. On a pure complementary energy principle and a force-based finite element formulation for non-linear elastic cables. Int. J. Non-Linear Mech. 46, 395–406.

Schwarz, U.S., Safran, S.A., 2013. Physics of adherent cells. Rev. Mod. Phys. 85, 1327–1381.

Shemesh, T., Geiger, B., Bershadsky, A.D., Kozlov, M.M., 2005. Focal adhesions as mechanosensors: A physical mechanism. Proc. Natl. Acad. Sci. 102 (35), 12383–12388.

Soheilypour, M., Peyro, M., Peter, S.J., Mofrad, M.R.K., 2015. Buckling behavior of individual and bundled microtubules. Biophys. J. 108 (7), 1718–1726.

Stamenović, D., Ingber, D.E., 2002. Models of cytoskeletal mechanics of adherent cells. Biomech. Model. Mechanobiol. 1, 95–108.

Stamenović, D., Ingber, D.E., 2009. Tensegrity-guided self assembly: From molecules to living cells. Soft Matter 5 (6), 1137–1145.

Stehbens, S.J., Wittmann, T., 2014. Analysis of focal adhesion turnover: A quantitative live-cell imaging example. In: Waters, Jennifer C., Wittman, Torsten (Eds.), Quantitative Imaging in Cell Biology. In: Methods in Cell Biology, vol. 123, Academic Press, pp. 335–346.

Tanaka, E., Kirschner, M.W., 1995. The role of microtubules in growth cone turning at substrate boundaries. J. Cell Biol. 128 (1), 127–137.

Wang, N., Naruse, K., Stamenović, D., Fredberg, J.J., Mijailovich, S.M., Tolić-Nørrelykke, I.M., Polte, T., Mannix, R., Ingber, D.E., 2001. Mechanical behavior in living cells consistent with the tensegrity model. Proc. Natl. Acad. Sci. 98 (14), 7765–7770.

Wang, N., Tolić-Nørrelykke, I.M., Chen, J., Mijailovich, S.M., Butler, J.P., Fredberg, J.J., Stamenović, D., 2002. Cell prestress. I. Stiffness and prestress are closely associated in adherent contractile cells. Am. J. Physiol. Cell Physiol. 282 (3), C606–C616.

Wehrle-Haller, B., Imhof, B.A., 2002. The inner lives of focal adhesions. Trends Cell Biol. 12 (8), 382–389.

Yip, A.K., Iwasaki, K., Ursekar, C., Machiyama, H., Saxena, M., Chen, H., Harada, I., Chiam, K.H., Sawada, Y., 2013. Cellular response to substrate rigidity is governed by either stress or strain. Biophys. J. 104 (1), 19–29.